

Non-equilibrium dynamics in heavy ion collisions at low SIS energies

Qingfeng Li^{1a}, Caiwan Shen¹, Chenchen Guo^{1,2}, Yongjia Wang^{1,3}, Zhuxia Li⁴, J. Lukasik^{5,6}, and W. Trautmann⁵

1) School of Science,

Huzhou Teachers College,

Huzhou 313000, P.R. China

2) College of Physics Science & Technology,

Shenyang Normal University,

Shenyang 110034, P.R. China

3) School of Nuclear Science and Technology,

Lanzhou University,

Lanzhou 730000, P.R. China

4) China Institute of Atomic Energy,

Beijing 102413, P.R. China

5) GSI Helmholtzzentrum für Schwerionenforschung GmbH,

D-64291 Darmstadt, Germany

6) H. Niewodniczański Institute of Nuclear Physics,

Pl-31342 Kraków, Poland

arXiv:1101.5661v1 [nucl-th] 29 Jan 2011

^a E-mail address: liqf@hutc.zj.cn

Abstract

The Ultrarelativistic Quantum Molecular Dynamics (UrQMD) model, a microscopic transport model, is used to study the directed and elliptic collective flows and the nuclear stopping in Au+Au collisions at incident energies covered by INDRA and lower-energy FOPI experiments. It is seen clearly that these observables are sensitive to both, the potential terms (including iso-scalar and iso-vector parts as well as the momentum dependent term) in the equation of state (EoS) and the collision term (including the Pauli-blocking and the medium-modified nucleon-nucleon elastic cross section (NNECS)). The momentum modifications of both, the mean-field potentials and the density dependent NNECS, are found to be sensitive to the collectivity of heavy-ion collisions. At INDRA energies (≤ 150 MeV/nucleon), the dynamic transport with a soft EoS with momentum dependence and with the momentum-modified density-dependent NNECS describes the directed flow exhibited by hydrogen isotopes ($Z = 1$) emitted at mid-rapidity fairly well.

PACS numbers: 25.70.-z,24.10.-i,25.75.Ld

I. INTRODUCTION

Nuclear reactions at intermediate energies as, e.g., provided by the heavy-ion synchrotron SIS at GSI have been investigated for several decades but the physics governing their mechanisms are not yet thoroughly understood and further investigations seem necessary. Recently the two experimental collaborations INDRA and FOPI have published a series of systematic observations made in experiments at the GSI laboratory regarding several physical quantities such as the collective flows, the nuclear stopping, and the light cluster and produced-particle, i.e. mostly pion, production [1–4]. Comparisons with model calculations (mainly performed with the Quantum Molecular Dynamics (QMD) model), revealed some discrepancies which deserve deeper investigations, mainly concerning dynamical observables. The excitation functions of the directed and elliptic collective flows and the nuclear stopping cannot be satisfactorily described with the same equation of state (EoS) of nuclear matter (see e.g. [5, 6]).

Important progress in nuclear physics at intermediate energies was made recently by reaching consensus on the soft nature of the EoS of nuclear matter [5, 7–10]. However, according to the theory of quantum hydrodynamics (QHD), both the mean field and the two-body collisions have the same origin, the effective Lagrangian density, based on which the medium modifications of both the collisions and the mean-field transport between the collisions should be considered self-consistently [11–15]. More explicitly, the medium-modified terms should take the density dependence, the isospin asymmetry, and the momentum constraints into account. In past investigations, these medium effects were considered mainly in the mean-field part but usually not in the collision part, leading to an obvious lack of self-consistency. Hence, conclusions based on these treatments are not fully reliable, and it is easy to understand why new difficulties arose in the recent comparisons of data with model calculations.

In the lower range of SIS energies, the collision rate is known to increase with beam energy and the interplay between mean field and two-body collisions leads to a colorful phenomenology of the nuclear dynamics as, e.g., apparent in the excitation functions of collective flows [2–4, 16–18]: with the increase of beam energy beyond the INDRA range (≤ 150 MeV/nucleon), the slope, near mid-rapidity and with respect to rapidity, of the directed flow of free protons or light clusters changes sign from negative to positive, while the value

of the elliptic flow at mid-rapidity changes from positive (in-plane) to negative (squeeze-out). These transitions of the directed and elliptic flows imply clearly that the strength of two-body collisions and the nuclear stopping power increase, which has been observed in recent INDRA experiments as well [1, 2, 19]. Theoretically, in addition to the well-known density-dependent modifications of binary cross sections, the momentum constraints will have to be considered seriously in order to describe these data systematically [20–31].

In our previous work, we have attempted to build up a microscopic transport model in which the dynamic process of heavy ion collisions (HICs) is described in a more consistent and complete manner. The Ultrarelativistic Quantum Molecular Dynamics (UrQMD) model is adopted as a microscopic transport basis [32–34]. In Refs. [35–38], both the mean-field potentials and the relativistic effects on the relative distance and momentum in potentials are treated comprehensively. In Refs. [26, 28], the medium modifications of the nucleon-nucleon elastic cross sections (NNECS) are further taken into account. With the so improved version of the UrQMD model, several experimental observables at SIS and AGS energies were successfully described [37–42]. With the further consideration of the “pre-formed” hadron potentials, the well-known HBT time-related puzzle throughout the beam energy range from SIS up to RHIC is well understood [43, 44]. It is also found, however, that further investigation is still needed at the lower SIS energies [40]. This will become evident in this work from the study of collective flows and nuclear stopping.

The paper is arranged as follows: Section II presents the new updates in the UrQMD transport model. Results for collective flows and nuclear stopping in the energy range covered by INDRA and FOPI experiments are then shown in Section III. Finally, a conclusion and an outlook are given in Section IV.

II. URQMD TRANSPORT MODEL AND UPDATES

The UrQMD model is based on analogous principles as the QMD model [45, 46] and the Relativistic Quantum Molecular Dynamics (RQMD) model [47]. The first formal version (ver1.0) of the UrQMD transport model was published at the end of last century [32, 33, 48]. Since then, a large number of successful theoretical analyses, predictions, and comparisons with data have been accomplished with this transport model for pp , pA and AA reactions and over a large range of beam energies, essentially from SIS over AGS, SPS, RHIC, up to

LHC energies [49].

A. Potential updates

In the UrQMD, similar to the QMD, hadrons are represented by Gaussian wave packets in phase space. After the initialization of projectile and target nuclei for which the Hard-Sphere (H-S) or the Woods-Saxon (W-S) mode may be selected, the phase space of hadron i is propagated according to Hamilton's equations of motion:

$$\dot{\mathbf{r}}_i = \frac{\partial H}{\partial \mathbf{p}_i}, \quad \text{and} \quad \dot{\mathbf{p}}_i = -\frac{\partial H}{\partial \mathbf{r}_i}. \quad (1)$$

Here \mathbf{r} and \mathbf{p} are the coordinate and momentum of hadron i . The Hamiltonian H consists of the kinetic energy T and the effective two-body interaction potential energy V ,

$$H = T + V, \quad (2)$$

with

$$T = \sum_i (E_i - m_i) = \sum_i (\sqrt{m_i^2 + \mathbf{p}_i^2} - m_i). \quad (3)$$

In the standard version of the UrQMD model [32, 33, 48], the potential energies include the two-body and three-body Skyrme-, and the Yukawa-, Coulomb-, and Pauli-terms as a base,

$$V = V_{sky}^{(2)} + V_{sky}^{(3)} + V_{Yuk} + V_{Cou} + V_{Pau}. \quad (4)$$

The three-body terms of the Skyrme force can be approximately written in the form of two-body interactions, the so-called density dependent terms. Only the Coulomb force between charged baryons is considered in the default version. However, when also considered for charged mesons it was found indispensable for reproducing certain observables [35, 38].

The single particle potential follows from $U = \delta V / \delta f$, where f is the phase-space Wigner distribution function which reads as

$$f(\mathbf{r}, \mathbf{p}) = \sum_i f_i(\mathbf{r}, \mathbf{p}) = \sum_i \frac{1}{(\pi\hbar)^3} e^{-(\mathbf{r}-\mathbf{r}_i)^2/2L^2} e^{-(\mathbf{p}-\mathbf{p}_i)^2 \cdot 2L^2/\hbar^2}, \quad (5)$$

where L is the width parameter of the wave packet. It is known that the width affects the stability of initialized nuclei and the production of clusters at later reaction stages [50].

Empirically, the value of the wave packet width should grow from about 1 fm to 2 fm as the total mass of the colliding system increases from light to heavy. As an example, for Au+Au collisions a value of $L = 2$ fm is chosen while for Ca+Ca and lighter nuclei $L = 1$ fm is found more appropriate.

Recently, in order to permit more successful applications in the intermediate energy regime ($0.1A \lesssim E_{lab} \lesssim 2A$ GeV), more potential terms have been incorporated into the UrQMD [37]. The first addition is the density-dependent average symmetry potential energy term $V_{sym}^{pot} \delta^2$, where $\delta = (\rho_n - \rho_p)/\rho_0$ is the isospin-asymmetry. In this work, the form

$$V_{sym}^{pot} = (S_0 - \frac{\epsilon_F}{3})u^\gamma \quad (6)$$

introduced in Ref. [51] is used. Here S_0 is the symmetry energy at the normal nuclear density ρ_0 , ϵ_F is the Fermi kinetic energy at normal nuclear density, $u = \rho/\rho_0$ is the reduced nuclear density, and γ is the strength of the density dependence of the symmetry potential. In this work, the value $S_0 = 34$ MeV is chosen. The symmetry potential is important for isospin-asymmetric reactions at intermediate and low energies since the uncertainties existing in the symmetry energy based on various theories were found to be large at densities away from the normal density [52]. Here, a soft ($\gamma = 0.5$) density dependent symmetry potential is adopted. Recent investigations indicate that the density dependence of the symmetry energy at subnormal densities might be soft [29, 53, 54]. However, this will still have to be confirmed by further studies.

The second addition is the momentum-dependent term [55]

$$U_{md} = t_{md} \ln^2[1 + a_{md}(\mathbf{p}_i - \mathbf{p}_j)^2] \rho_i/\rho_0, \quad (7)$$

where $t_{md} = 1.57$ MeV and $a_{md} = 500$ c²/GeV² are selected as in previous calculations within the QMD family. It has to be noted, however, that this form may also have to be refined in order to obtain improved fits of the real part of the optical potential [8, 56].

At beam energies higher than the AGS regime, potentials for “pre-formed” particles (string fragments) and relativistic effects regarding the relative distance and the relative momentum employed in the two-body potentials (Lorentz transformation) are, furthermore, considered [38, 43]. They can be neglected in this work here.

B. New Pauli-blocking treatment for two-body collision

Regarding the collision term, it is well-known that the rate of collisions is reduced by the quantum Pauli-blocking. However, in the default version of the UrQMD, for simplicity, the Pauli-blocking criteria are realized with an algorithm based on fitted parameters: for the same type of particles, the binary scattering will be blocked under the form

$$\eta < \psi, \quad (8)$$

where

$$\psi = \sum_i e^{-\frac{(\mathbf{r}-\mathbf{r}_i)^2}{4L^2}} e^{-\frac{(\mathbf{p}-\mathbf{p}_i)^2 \cdot L^2}{\hbar^2}}, \quad (9)$$

and

$$\eta = a_{fit} + b_{fit}\varrho \quad (10)$$

with

$$\varrho = \sum_i e^{-\frac{(\mathbf{r}-\mathbf{r}_i)^2}{2L^2}}. \quad (11)$$

The parameters a_{fit} and b_{fit} in Eq. (10) are set to be 1.49641 and 0.208736, respectively. It will be shown below that, for descriptions of experimental observables at the lower energies, the default Pauli-blocking treatment is not precise enough. Therefore, an updated new version of the Pauli-blocking routine is introduced here. For the same type of particles and for each collision, firstly, the phase space densities in the final states are determined in order to assure that they are in agreement with the Pauli principle and, secondly, the following two criteria are considered at the same time:

$$\frac{4\pi}{3}r_{ij}^3 \cdot \frac{4\pi}{3}p_{ij}^3 \geq (2s+1) \cdot \left(\frac{\hbar}{2}\right)^3 \quad (12)$$

and

$$P_{block} = 1 - (1 - f_i)(1 - f_j) < \xi. \quad (13)$$

On the left-hand side of Eq. (12), the r_{ij} and p_{ij} are the relative distance and momentum of the two particles at the final states i and j . The factor $(2s+1)$ on the right side of Eq. (12) denotes the summation of the spins of the two particles. In Eq. (13), ξ represents a random number between 0 and 1. If one of the criteria is not fulfilled the collision is not allowed and the two particles remain with their original momenta.

Set	λ	ζ
FU1	1/3	0.54568
FU2	1/4	0.54568
FU3	1/6	1/3

TABLE I. The three parameter sets FU1, FU2, and FU3 used for the density-dependent correction factor F_u of NNECS.

C. Medium modifications and momentum dependence of NNECS

It is also known that the cross sections will be modified by the nuclear medium, according to the QHD theory (see, e.g., Refs. [13–15, 23, 30, 31, 57, 58]. As in previous work, the in-medium NNECS σ_{el}^* are treated to be factorized as the product of a medium correction factor $F(u, \alpha, p)$ and the free NNECS σ_{el}^{free} [26]. For the inelastic channels, we still use the experimental free-space cross sections σ_{in}^{free} . It is believed that this assumption does not have strong influence on our present study at low SIS energies. Therefore, the total two-body scattering cross section of nucleons, σ_{tot}^* , will be modified according to

$$\sigma_{tot}^* = \sigma_{in} + \sigma_{el}^* = \sigma_{in}^{free} + F(u, \alpha, p)\sigma_{el}^{free}. \quad (14)$$

As for the medium correction factor $F(u, \alpha, p)$, it is proportional to both the isospin-scalar density effect F_u and the isospin-vector mass-splitting effect F_α . Studies of the isospin-related splitting effect on NNECS which is represented by the F_α factor have been reported in Refs. [26, 28].

Furthermore, the factors F_u and F_α should be functions of the relative momentum p_{NN} of the two colliding particles in the NN center-of-mass system. In Ref. [26], they are formulated as

$$F_{\alpha,u}^p = \begin{cases} f_0 & p_{NN} > 1\text{GeV}/c \\ \frac{F_{\alpha,u}-f_0}{1+(p_{NN}/p_0)^\kappa} + f_0 & p_{NN} \leq 1\text{GeV}/c. \end{cases} \quad (15)$$

The factor F_u can be expressed as

$$F_u = \lambda + (1 - \lambda) \exp[-u/\zeta]. \quad (16)$$

Set	f_0	p_0 [GeV c ⁻¹]	κ
FP1	1	0.425	5
FP2	1	0.225	3
FP3	1	0.625	8
no p_{NN} limit	$F(u)$	/	/

TABLE II. The three parameter sets FP1, FP2, and FP3 used for describing the momentum dependence of F_u . The fourth case, without a p_{NN} limit, is obtained by setting f_0 equal to $F(u)$ in Eq. (15).

Here ζ and λ are parameters which determine the density dependence of the cross sections. In this work, we select several parameter sets which are shown in Table I and illustrated in the left panel of Fig. 1. The reduction of the NNECS as a function of density becomes increasingly more pronounced as the parameterization is changed from FU1 to FU3. At the reduced density $u = 2$, e.g., the values of FU1, FU2, and FU3 are 0.35, 0.27, and 0.17, respectively. We note here that the density dependence of the FU1 parameterization is in qualitative agreement with previous work based on the Dirac-Brueckner approach [30, 31, 59]. However, in our previous investigations of the NNECS, based on the effective Lagrangian of density-dependent relativistic hadron theory in which the σ , ω , ρ and δ [$a_0(980)$] mesons are included [23], it was shown that especially the neutron-proton cross sections $\sigma_{el,np}^*$ might be largely reduced in the neutron-rich nuclear medium; the corresponding reduction factor might be as low as ~ 0.1 at $u = 2$. Therefore, the other parameter sets FU2 and FU3 (Table I) are still to be considered reasonable assumptions.

The parameters f_0 , p_0 and κ in Eq. (15) can be varied in order to obtain various momentum dependences of F_u . In this work, we select several parameter sets which are shown in Table II. The corresponding F_u^p functions are illustrated in the right panel of Fig. 1 for FU1 at a reduced density $u = 2$. The FP1 set was used in our previous work in which the medium modifications of cross sections were considered [26]. The parameterizations FP2 or FP3 result in a rise of the correction factor F at smaller or at larger p_{NN} than obtained with FP1. It illustrates the present uncertainty associated with treating the momentum dependence of the density-dependent cross sections. With a certain set of isospin dependent

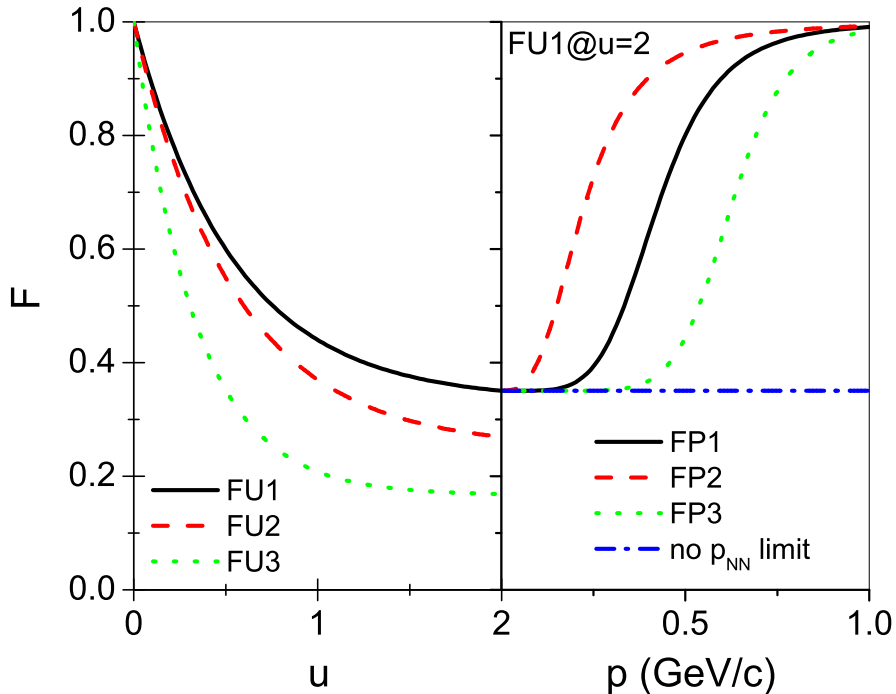


FIG. 1. (Color online) Correction factor F obtained with the parameterizations FU1, FU2, and FU3 given in Table I (left panel) and the momentum dependence obtained with the four options FP1, FP2, FP3, and “no p_{NN} limit” given in Table II for the example of FU1 at $u = 2$ (right panel).

EoS, the NNECS might even be enhanced at large momenta, in comparison to the cross sections at free space. It arises from the differences between the isoscalar and isovector channels[15]. An indication of this enhancement was obtained from a recent calculation of flow observables by Zhang *et al.* [20]. But it will not be discussed in the current work since the effect is related to collisions at large p_{NN} and it becomes increasingly important for heavy-ion collisions at higher beam energies. And, for completeness, the case without any momentum constraint on F_u (“no p_{NN} limit”) is listed in Table II.

III. CALCULATIONS AND OBSERVABLES

A. Colliding system and the after-burner

About 120 thousand events of $^{197}\text{Au}+^{197}\text{Au}$ collisions for each of the energies $E_{lab} = 40, 50, 60, 80, 100, 150,$ and 400 MeV/nucleon are calculated randomly within the impact parameter region 0-7.5 fm. For each beam energy, the calculations are divided into three groups according to impact parameter representing the central (0-2 fm), the semi-central (2-5.5 fm), and the semi-peripheral (5.5-7.5 fm) group of collisions. Fourteen parameterizations of the UrQMD transport model differing in the treatments of the Pauli-blocking of two-body collisions (P-B), of the potential terms (EoS), of the medium-modified NNECS with the density-dependent factor F_u and the momentum modification F^p of F_u , and of the initialization (ini.) are shown in Table III and will be discussed in the following section. The UrQMD transport program stops and produces the output after a collision time of 150 fm/c. Several more outputs are produced, as the calculations evolve, at different reaction times before the stop time. For each output, a conventional phase-space coalescence model [60] with two parameters is used to construct clusters. Nucleons with relative momenta smaller than P_0 and relative distances smaller than R_0 are considered to belong to one cluster. In this work, P_0 and R_0 are chosen to be 0.2 GeV/c and 2.8 fm, respectively. It is evident and well-known that the criteria chosen for constructing clusters affect their yields and, consequently, also related observables [61].

B. Collective flows and the stopping *vartl*

In this work, we will focus on the parameters describing the strength and orientation of directed and elliptic collective flows defined as

$$v_1 \equiv \langle \cos(\phi - \Phi_{RP}) \rangle = \langle \frac{p_x}{p_t} \rangle, \quad (17)$$

and

$$v_2 \equiv \langle \cos[2(\phi - \Phi_{RP})] \rangle = \langle \frac{p_x^2 - p_y^2}{p_t^2} \rangle. \quad (18)$$

Here ϕ denotes the azimuthal angle of the considered outgoing particle; Ψ_{RP} is the azimuthal angle of the reaction plane which is pre-configured in the calculations, $\Psi_{RP} = 0$, but has to be

Set	P-B	EoS	F_u	F^p	ini.
UrQMD-0	default	SM	FU1	FP1	H-S
UrQMD-I	new	SM	FU1	FP2	H-S
UrQMD-II	new	SM	FU1	FP1	H-S
UrQMD-III	new	SM	FU1	FP1	W-S
UrQMD-IV	new	Cascade	FU1	FP1	W-S
UrQMD-V	new	SM(no $V_{sym}+V_{Cou}$)	FU1	FP1	H-S
UrQMD-VI	new	SM	no Collisions	no Collisions	H-S
UrQMD-VII	new	SM	FU1	FP3	H-S
UrQMD-VIII	new	SM	FU1	no p_{NN} limit	H-S
UrQMD-IX	new	S	FU1	FP1	H-S
UrQMD-X	new	S	FU1	no p_{NN} limit	H-S
UrQMD-XI	new	S	FU2	no p_{NN} limit	H-S
UrQMD-XII	new	S	FU3	no p_{NN} limit	H-S
UrQMD-XIII	new	SM	FU3	FP1	H-S

TABLE III. Fourteen parameterizations of the UrQMD transport model differing in the treatments of the Pauli-blocking of two-body collisions (P-B), of the potential terms (EoS), of the medium-modified NNECS with the density-dependent factor F_u and the momentum modification F^p of F_u , and of the initialization (ini.). See text for details.

determined in experiments; p_x and p_y are the two components of the transverse momentum $p_t = \sqrt{p_x^2 + p_y^2}$. The angular brackets denote an average over all considered particles from all events.

The nuclear stopping is described with the quantity $vartl$ [62] defined as

$$vartl = \frac{\Gamma_{dN/dy_x}}{\Gamma_{dN/dy_z}}. \quad (19)$$

Here

$$\Gamma_{dN/dy_{x,z}} = \langle y_{x,z}^2 \rangle = \frac{\sum (y_{x,z}^2 N_{y_{x,z}})}{\sum N_{y_{x,z}}}, \quad (20)$$

where Γ_{dN/dy_x} and Γ_{dN/dy_z} are the variances of the rapidity distributions of fragments in the x and z directions, respectively. They are obtained as weighted averages of y^2 over the considered ranges in rapidity with N_{y_x} and N_{y_z} denoting the yields of fragments in each of the y_x and y_z rapidity bins.

Directed and elliptic flows and the nuclear stopping quantity v_{rtl} were measured by the INDRA and FOPI collaborations at GSI/Darmstadt [1–4]. In the following, the predictions of the UrQMD model for these observables will be analyzed, while the directed flow is chosen for the comparison with the experimental data at INDRA energies ($E_{lab} \leq 150$ MeV/nucleon).

IV. RESULTS

A. Pauli-Blocking effects on flows

As stated before, the Pauli-blocking treated in the default UrQMD model is an effective one. The advantage of this treatment is the high-speed to calculate it. However, it is found that it is not quite suitable for nuclear reactions at low SIS energies. In Fig. 2 we present the reduced longitudinal rapidity distribution of directed (v_1 , top plots) and elliptic (v_2 , bottom plots) flows of free protons from semi-peripheral ($b=5.5-7.5$ fm) Au+Au collisions at $E_{lab} = 40, 80, \text{ and } 400$ MeV/nucleon. The calculations with the default treatment of Pauli-blocking used in UrQMD-0 and with the new treatment incorporated in UrQMD-II (the only difference between the two versions, cf. Table III) are shown in Fig. 2.

Considerable differences exist in the rapidity distribution of both flow parameters at the lower SIS energies $E_{lab} = 40$ and 80 MeV/nucleon. With the default treatment, the slope of v_1 is significantly positive at mid-rapidity and the value of v_2 is rather small. Experimentally it is known that the slope of the directed flow of $Z = 1$ particles from semi-central/peripheral collisions of heavy systems at 40 MeV/nucleon is slightly negative at mid-rapidity and that the elliptic flow is positive with values near $v_2 = 0.08$ [1], values much closer to the results obtained with the new treatment of Pauli-blocking (Fig. 2, left panels). It is, therefore, concluded that this modification of the UrQMD is more suitable for this energy range,

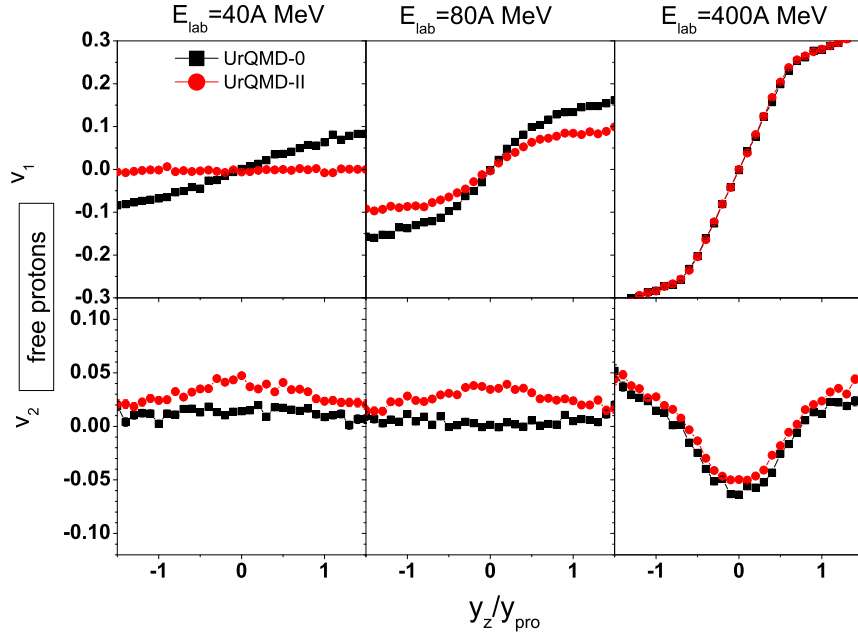


FIG. 2. (Color online) Parameters v_1 of directed flow (top panels) and v_2 of elliptic flow (bottom panels) for free protons from semi-peripheral ($b = 5.5 - 7.5$ fm) $^{197}\text{Au} + ^{197}\text{Au}$ collisions at $E_{\text{lab}} = 40$ (left), 80 (middle), and 400 MeV/nucleon (right), calculated with the versions UrQMD-0 (squares) and UrQMD-II (circles), as a function of the reduced rapidity y_z/y_{pro} .

and the new treatment of Pauli-blocking is chosen for the following investigations. The differences start to disappear at the higher energy 400 MeV/nucleon (right panels of Fig. 2).

B. Causes of collective phenomena

In order to understand how the initialization, the mean-field potentials and collisions influence collective flows, calculations were performed with the versions UrQMD-II, UrQMD-III, UrQMD-IV, UrQMD-V, and UrQMD-VI (Fig. 3). Several interesting phenomena are observed: comparing first the results obtained with UrQMD-II and UrQMD-III which differ only in the initialization, small differences are seen but the directed flow is slightly less positive at 40 MeV/nucleon and slightly more positive at 80 MeV/nucleon with the Hard-Sphere treatment of UrQMD-II than with the Wood-Saxon initialization of UrQMD-III. This is due to the fact that at 40 (80) MeV/nucleon the net-contribution of both mean-field potentials and two-body collisions is more attractive (positive) and the Hard-Sphere

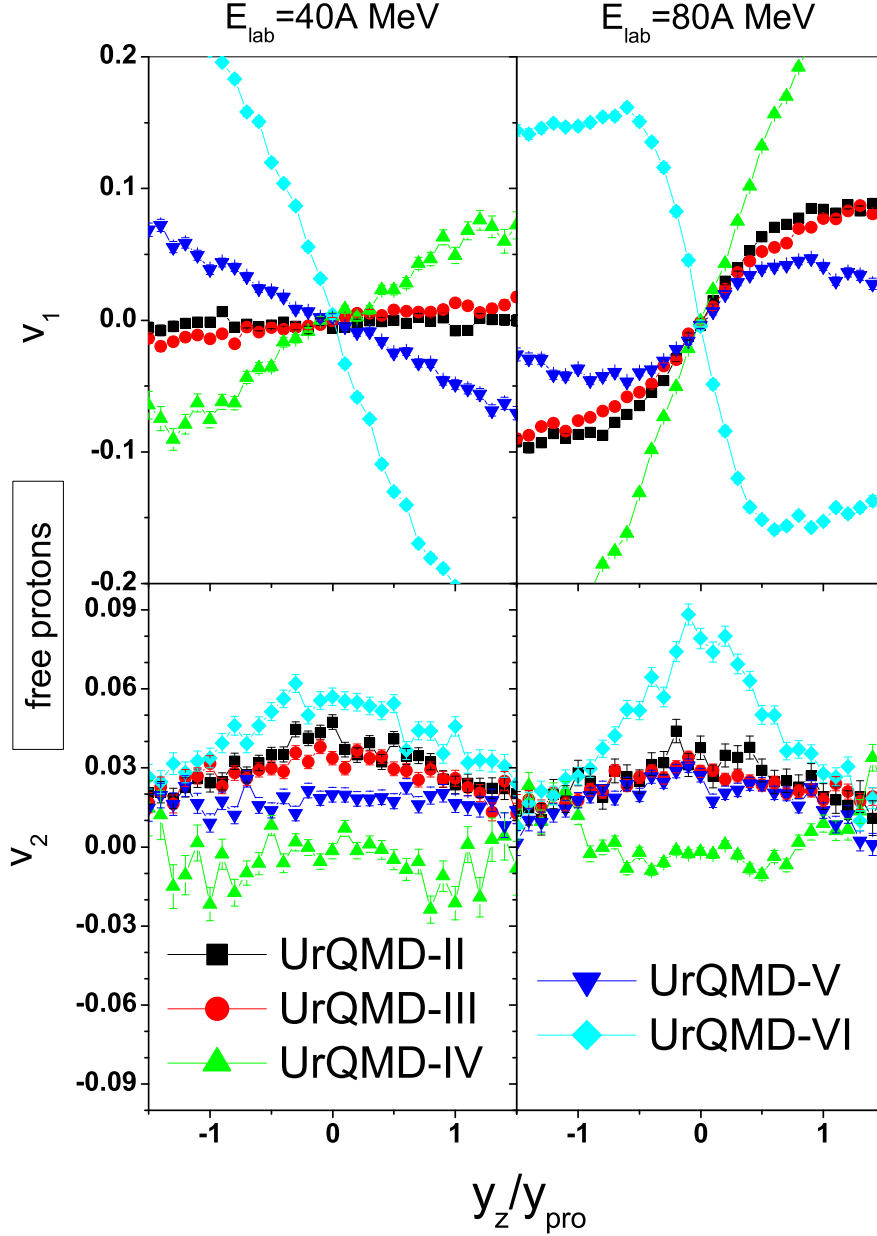


FIG. 3. (Color online) Parameters v_1 of directed flow (top panels) and v_2 of elliptic flow (bottom panels) for free protons from semi-peripheral ($b = 5.5 - 7.5 \text{ fm}$) $^{197}\text{Au} + ^{197}\text{Au}$ collisions at $E_{\text{lab}} = 40$ (left) and 80 MeV/nucleon (right) as a function of the reduced rapidity y_z/y_{pro} . The calculations performed with versions UrQMD-II, UrQMD-III, UrQMD-IV, UrQMD-V, and UrQMD-VI (see Table III) are distinguished by their symbols as indicated.

initialization may lead to stronger attraction (repulsion). Actually, this effect of different initializations was seen before in calculations with the IQMD model [50]. Since its effect on final flows is very small, mainly the Hard-Sphere initialization will be used in the following calculations. It is the default initialization in the UrQMD model.

Secondly, if the mean-field potentials are ignored as in the cascade-type version UrQMD-IV, a large positive slope of v_1 is seen at both beam energies. It implies that the net contribution of the collision term to the directed flow is repulsive. The elliptic flow has almost vanished which should be due to both, a relatively weak contribution of the collision term and the almost isotropic differential NNECS. On the other hand, if the collision term is switched off and only the mean-field potentials are active as in UrQMD-VI, a strong negative directed flow is seen at both beam energies. The elliptic flow v_2 is largest in this case, indicating that the mean-field potentials contribute to the collective flows much more strongly than the collision term at lower SIS energies, a fact that is well-known. It is also found that the net contributions of the mean-field and of two-body collisions to the directed flow are attractive and repulsive, respectively. The positive elliptic flow induced by the mean-field is caused by the in-plane geometry at early reaction times.

The isospin-scalar and isospin-vector related parts of the potentials may yield different contributions to the final flows. This was tested with the results of UrQMD-II, UrQMD-IV, and UrQMD-V in which a soft-EoS with momentum dependence (SM-EoS, the corresponding incompressibility $K = 200$ MeV) is considered, not considered, and partially considered, respectively, while the same collision term is adopted. It is found that the iso-scalar part of the potentials produces a strong attractive force (comparison of UrQMD-IV and UrQMD-V) while the iso-vector related part gives a relatively weak repulsive force to the directed flow (see from UrQMD-V to UrQMD-II). The repulsion caused by the iso-vector potentials (symmetry and Coulomb potentials) is obvious since the Coulomb potential of protons is always repulsive and much stronger than the symmetry potential, regardless of whether the total effect of the symmetry term is attractive or repulsive. The latter depends on the isospin-asymmetry of the nuclear medium during the whole dynamic process of HICs.

Summarizing this analysis, one finds clearly that 1) the balance of contributions between mean-field potentials and the collision term determines the vanishing of the directed flow at low SIS energies with roughly equal strength; 2) in the mean-field potentials, the iso-scalar part behaves as an attractive effect which is due to the overall rather low densities of heavy-

ion collisions at such low beam energies. The iso-vector part is repulsive which is mainly due to the mutual Coulomb repulsion of the protons.

Another set of comparisons of flow results, calculated with versions UrQMD-I, UrQMD-II, UrQMD-VIII, and UrQMD-IX is shown in Fig. 4. Two beam energies 40 and 400 MeV/nucleon are selected. The comparison of UrQMD-I, UrQMD-II, UrQMD-VIII shows the effects on the flow parameters resulting from different momentum-modified NNECS while the comparison of UrQMD-II and UrQMD-IX shows those of the momentum-dependent terms in the potentials (with or without momentum dependence). It is, first of all, noticed that both effects, the momentum modification of the density-dependent NNECS in the collision term and the momentum dependence of the potentials affect both flow variables v_1 and v_2 . Secondly, when studied in more detail, these flow effects are found to behave differently at different beam energies: (1) regarding the contribution of medium-modified cross sections, we see that for the directed flow at 40 MeV/nucleon the difference is large between the UrQMD-I and UrQMD-II results, while at 400 MeV/nucleon the largest difference exists between the UrQMD-I and UrQMD-VIII results. It is obviously caused by the difference of the momentum modifications of cross sections (FP1, FP2, and no P_{NN} limit) as they appear at different energies; (2) for the elliptic flow at 40 MeV/nucleon, a difference is seen between the UrQMD-VIII and UrQMD-IX results, while this is no longer the case at 400 MeV. It implies that, at 40 MeV/nucleon, the momentum-dependent term in the potentials is more important than the momentum modification of the density dependent NNECS. They become equally important at 400 MeV/nucleon.

A rough comparison of the calculations with INDRA and FOPI data for $Z = 1$ particles from the same system shows that the effect of the momentum-dependent terms in the potentials is repulsive, i.e. not suitable for describing the measured negative slope of the v_1 flow and the largely positive v_2 (in-plane flow) at mid-rapidity and at the beam energy 40 MeV/nucleon. At 400 MeV/nucleon, the consideration of the momentum dependence in both, the mean-field and collision terms, is important to describe the measured largely positive slope of v_1 and largely negative v_2 (squeeze-out) at mid-rapidity. Therefore, the uncertainties existing in the momentum modification of NNECS will largely influence the excitation functions of flows, even only at low SIS energies.

The yield distributions of free protons as functions of the reduced longitudinal (y_z/y_{pro}) and transverse (y_x/y_{pro}) rapidities from central Au+Au collisions at $E_{\text{lab}} = 80$ MeV/nucleon

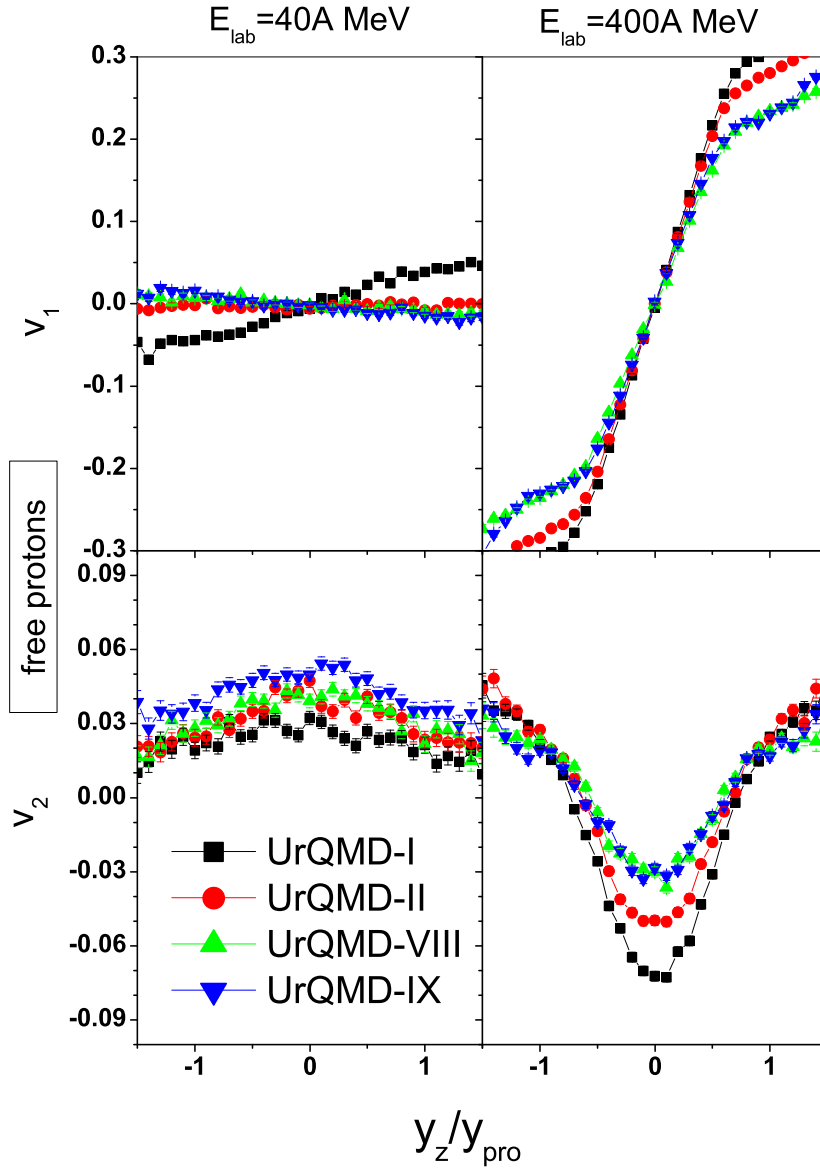


FIG. 4. (Color online) Parameters v_1 of directed flow (top panels) and v_2 of elliptic flow (bottom panels) for free protons from semi-peripheral ($b = 5.5 - 7.5$ fm) $^{197}\text{Au} + ^{197}\text{Au}$ collisions at $E_{\text{lab}} = 40$ (left) and 400 MeV/nucleon (right) as functions of the reduced rapidity y_z/y_{pro} . The calculations performed with versions UrQMD-I, UrQMD-II, UrQMD-VIII, and UrQMD-IX (see Table III) are distinguished by their symbols as indicated.

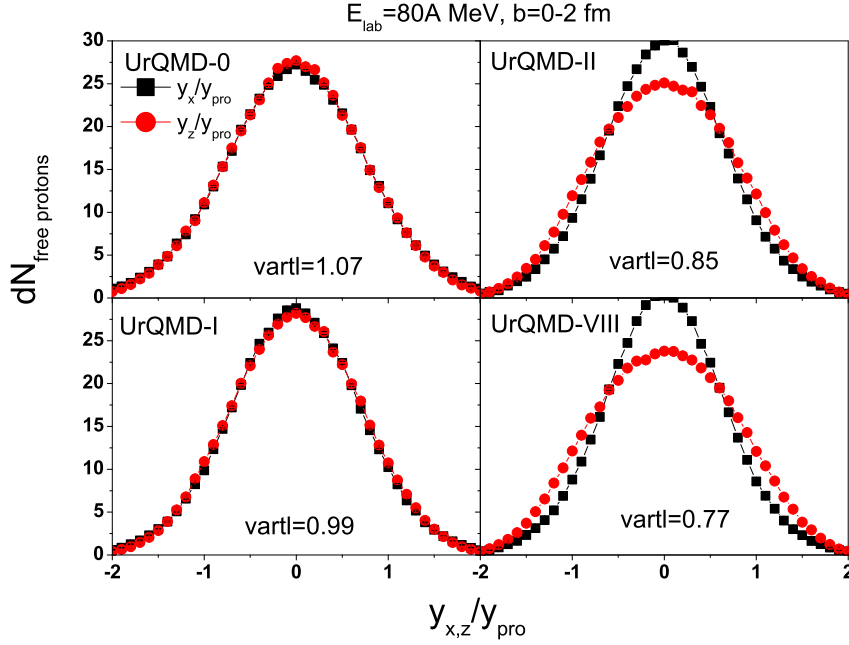


FIG. 5. (Color online) Yield distributions of free protons as functions of the reduced longitudinal (y_z/y_{pro} , squares) and transverse (y_x/y_{pro} , circles) rapidities from central ($b = 0 - 2$ fm) $^{197}\text{Au} + ^{197}\text{Au}$ collisions at $E_{\text{lab}} = 80$ MeV/nucleon. Calculations with UrQMD-0, UrQMD-I, UrQMD-II, and UrQMD-VIII (see Table III) are shown in the top-left, bottom-left, top-right, and bottom-right panels, respectively. The corresponding values obtained for the stopping observable $vartl$ for free protons are also indicated in each panel.

are shown in Fig. 5. Calculations with the default Pauli-blocking treatment in UrQMD-0 (top-left) are compared to those with the new Pauli-blocking treatment combined with the same (UrQMD-II, top-right) or alternative momentum modifications of NNECS (UrQMD-I, bottom-left and UrQMD-VIII, bottom-right). The corresponding values of $vartl$, for the full range of rapidities, are also given for each of the UrQMD versions. We first notice that, in the UrQMD-0 mode, the relative maximum of the proton yield is higher at mid-longitudinal-rapidity than at mid-transverse-rapidity, which leads to $vartl > 1$. In contrast, calculations with the new treatment of the Pauli-blocking, despite of uncertainties in the cross sections, the values of $vartl$ are always smaller than unity, in line with the experimental data.

Secondly, with decreasing cross sections (the reduction of NNECS due to the momentum modifications increases successively going from UrQMD-I to UrQMD-II and UrQMD-VIII),

the calculated values of v_{artl} become smaller and approach the experimental value 0.80 ± 0.03 [6] measured with INDRA at $E_{lab} = 80$ MeV/nucleon (note, however, that one can not compare directly with data since the experimentally selected clusters ($Z \leq 3$) and rapidity bins are different from the current calculations performed for $Z = 1$ particles). Together with the flow results shown in Fig. 4, these comparisons clearly show that the momentum modification of NNECS are important for describing the collective flows and the nuclear stopping at the low SIS energies at the same time. Thirdly, in the analyses related to Figs. 3, 4, and 5, one finds that the results for flows and for the nuclear stopping always follow in the same order when different treatments of the mean-field and the collisions terms are chosen. It, therefore, seems sufficient to select one of the observables, the slope of the directed flow at mid-rapidity, for the following more precise comparison with experimental data.

C. Comparison of the excitation function of the v_1 slope with INDRA data

A modification of the density dependence might be considered as an additional alternative to the momentum modification of NNECS in order to achieve their stronger reduction in heavy-ion collisions at lower energies and a weaker reduction at higher energies. In the left half of Fig. 6, we show values of the slope of directed flow at mid-rapidity ($|y_z/y_{pro}| < 0.4$) for $Z = 1$ particles from semi-central ($b = 2 - 5.5$ fm) Au+Au collisions at $E_{lab} = 40$ MeV/nucleon. Calculations with UrQMD-VI, UrQMD-X, UrQMD-XI, and UrQMD-XII are compared to the INDRA data. When the collision term is turned off (UrQMD-VI), the absolute value of the v_1 slope is larger than the data, indicating that collisions start to become important for heavy-ion collisions at such low beam energies. When the collision term is present and larger reductions of NNECS are considered by choosing UrQMD-X, UrQMD-XI, and UrQMD-XII (with increasingly larger density dependence but without momentum modification), the obtained v_1 slopes clearly approach the measured INDRA value.

On the right side of Fig. 6, again values of the slope of directed flow at mid-rapidity for $Z = 1$ particles from semi-central Au+Au collisions but for an incident energy $E_{lab} = 150$ MeV/nucleon are presented. Calculations with UrQMD-I, UrQMD-II, UrQMD-VII, and UrQMD-X are compared to the INDRA data. Obviously, with the increasingly weaker momentum modification of NNECS (as realized with UrQMD-I, UrQMD-II, and UrQMD-VII

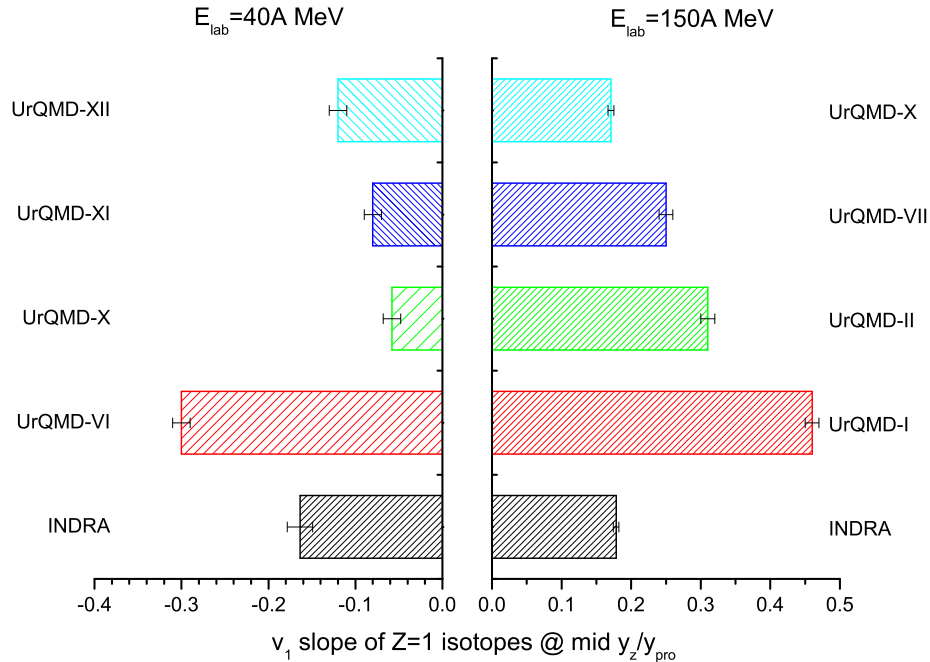


FIG. 6. (Color online) Values of the slope of directed flow at mid-rapidity ($|y_z/y_{pro}| < 0.4$) for $Z = 1$ particles from semi-central ($b = 2-5.5 \text{ fm}$) $^{197}\text{Au}+^{197}\text{Au}$ collisions at $E_{lab} = 40 \text{ MeV/nucleon}$ (negative values, left) and 150 MeV/nucleon (positive values, right). The INDRA results at both beam energies are compared with UrQMD calculations performed with the indicated versions (see Table III), all represented by the bars with different shadings.

in that sequence), the large reduction induced by the density dependence of the NNECS is less compensated, leading to a weaker repulsion and, hence, to the decreasing value of the v_1 slope shown in the figure. Alternatively, if we switch off both the momentum-dependent term in the potentials and the momentum modification of NNECS in the collision term, realized with the UrQMD-X calculation, the value of the v_1 slope is pushed down further and approaches the INDRA data. As a result of these tests, one may reach a deeper understanding of the difficulties in theoretically describing experimental data and of the importance of treating self-consistently the dynamic process of heavy-ion collisions. Furthermore, it is evident from Fig. 6 that even the version UrQMD-X is still not good enough to permit the description of the directed flow over the whole range of INDRA energies. Further refinements and tests will be needed.

The time evolution of the slope of directed flow at mid-rapidity for $Z = 1$ particles from

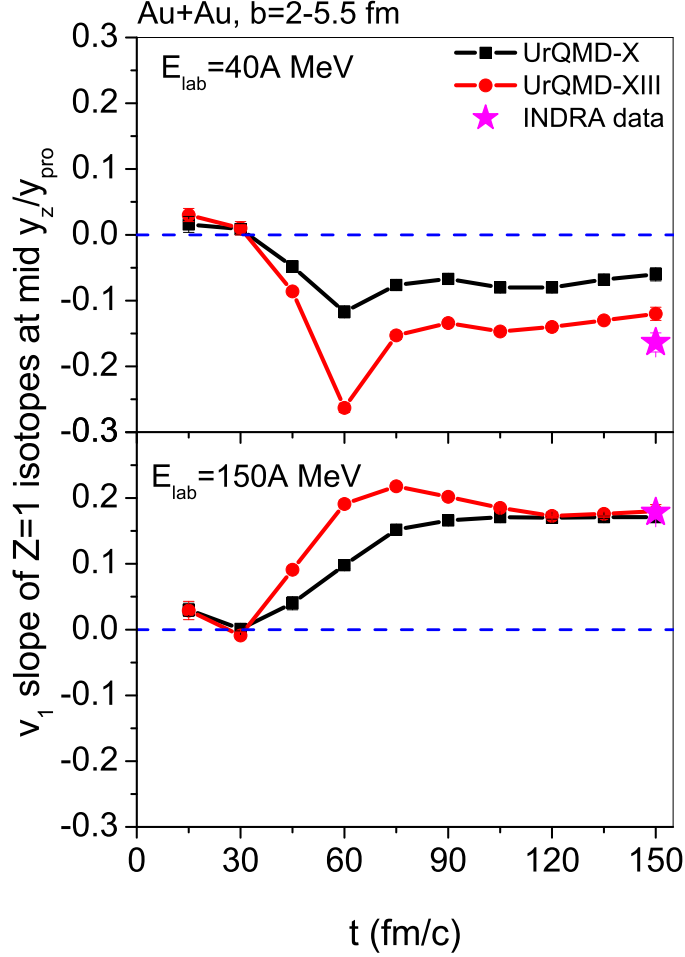


FIG. 7. (Color online) Time evolution of the slope of directed flow at mid-rapidity ($|y_z/y_{\text{pro}}| < 0.4$) for $Z = 1$ particles from semi-central ($b = 2 - 5.5$ fm) $^{197}\text{Au}+^{197}\text{Au}$ collisions at $E_{\text{lab}} = 40$ MeV/nucleon (top) and 150 MeV/nucleon (bottom). Calculations with UrQMD-X and UrQMD-XIII (see Table III) are represented by the squares and circles, respectively. The INDRA results for both beam energies are indicated by the stars positioned at the UrQMD stop time of 150 fm/c. The dashed horizontal lines representing zero slopes are included for comparison.

semi-central Au+Au collisions at $E_{\text{lab}} = 40$ (top) and 150 MeV/nucleon (bottom) are shown in Fig. 7. The versions chosen for the comparison are UrQMD-X, closest to the INDRA data at 150 MeV/nucleon (Fig. 6), and UrQMD-XIII. The latter differs from UrQMD-XII, closest to the data at 40 MeV/nucleon, in that the SM-EoS and the FP1 momentum modification of NNECS (the standard in previous investigations [26]) are adopted and from UrQMD-X

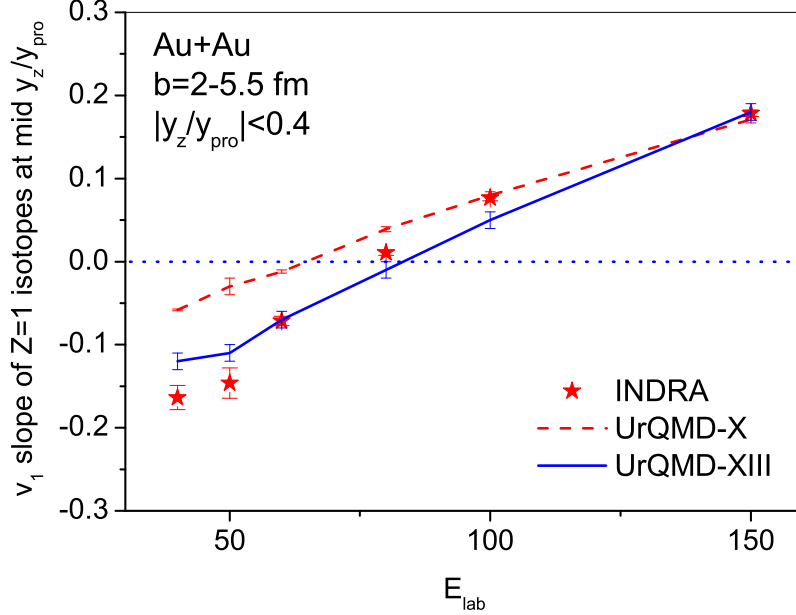


FIG. 8. (Color online) Excitation function of the slope of directed flow at mid-rapidity ($|y_z/y_{pro}| < 0.4$) for $Z = 1$ particles from semi-central ($b = 2 - 5.5$ fm) $^{197}\text{Au}+^{197}\text{Au}$ collisions in the range of INDRA energies from 40 to 150 MeV/nucleon. Calculations with UrQMD-X (dashed) and UrQMD-XIII (full line) are compared with the INDRA data (stars). The dotted horizontal line representing the zero slope is included for comparison.

by the stronger density dependence FU3 for NNECS (same as in UrQMD-XII). At about $t < 30$ fm/ c , the pre-equilibrated protons are emitted with a small positive flow due to the initial geometry. With increasing time, up to about 60 fm/ c , the value of the v_1 slope increases or decreases, depending on the balance between strong attractive and repulsive effects on particles during the rescattering process. At 40 MeV/nucleon, the net contribution is attractive, whereas at 150 MeV/nucleon it is repulsive, leading to the corresponding negative and positive flows. After 60 fm/ c , the final-state interactions (FSI) still affect the collisions at the low beam energy 40 MeV/nucleon, and the contributions of two-body scatterings start to become stronger than those of the mean field potentials. It is found that, although the FSI affects the final flow results, the UrQMD-X can not describe well the data at 40 MeV/nucleon. The UrQMD-XIII calculations can describe reasonably well both results at 40 and 150 MeV/nucleon.

Finally, in Fig. 8, the excitation function of the slope of directed flow at mid-rapidity for $Z = 1$ particles from semi-central Au+Au collisions is shown for the range of INDRA energies from 40 to 150 MeV/nucleon. The data are from Ref. [2] and compared to the results obtained with the same UrQMD-X and UrQMD-XIII whose time evolution has just been discussed. It is seen clearly that the UrQMD-XIII calculations describe the data well over the whole energy range including the location of the transition energy which is closely reproduced. It has to be noticed, however, that, in the energy range 90-150 MeV/nucleon covered also by FOPI experiments, the FOPI result for the v_1 slope of $Z = 1$ particles is higher by up to 0.05 than the INDRA data [2]. Thus, in order to pin down the exact form of the medium modifications on both the mean-field potentials and the collision terms, it will also be necessary to further reduce remaining uncertainties on the experimental side

V. CONCLUSIONS AND OUTLOOK

In summary, by using the microscopic transport model UrQMD, we have performed a systematic investigation on the effects of the momentum dependence of the mean field and the corrections from various aspects in the collision term, especially the modification of the density and momentum dependence of nucleon-nucleon elastic cross sections (NNECS) on the observables, such as the directed and elliptic flow and the stopping in HICs at low SIS energies. It is clearly seen that the collective flows and the nuclear stopping are sensitive to all these effects, meaning that they are important to the non-equilibrium dynamic process in HICs at low SIS energies.

Further, in order to describe experimental observables systematically, a consistent consideration of the uncertainties associated with both, the mean-field and the two-body collisions, is extremely important and should be paid more attention. The momentum dependence of the mean field potentials and of the density-dependent NNECS is found to be sensitive to the collectivity exhibited by the collision dynamics of HICs. At INDRA energies (40-150 MeV/nucleon), the dynamic transport with a soft equation-of-state with momentum dependence (SM-EoS) and with momentum-dependent and density-modified NNECS ($\sigma_{el}^*(\rho, p_{NN}, \delta)$) describes the slope of the directed flow of $Z = 1$ particles at mid-rapidity rather well.

From Ref. [2] we learned that the cluster charge-Z dependence of the transition energy

of flows has been discovered. However, the verification by the theoretical side is still absent since in many previous theoretical investigations the vanishing flow was studied with a cluster charge- Z *independent* global quantity — the so-called directed transverse momentum $\langle p_x^{dir} \rangle$. In addition, the isospin effect should be visible in (the time evolution and the excitation function of) collective flows at low SIS energies. The knowledge of the effect of isospin asymmetry on both the mean field and the NNECS might be renewed under the new version of the UrQMD. These studies are currently underway and will be addressed in a forthcoming paper.

ACKNOWLEDGEMENTS

We acknowledge support by the computing server C3S2 in Huzhou Teachers College. The work is supported in part by the key project of the Ministry of Education of China (No. 209053), the National Natural Science Foundation of China (Nos. 10905021,10979023, 10979024), the Zhejiang Provincial Natural Science Foundation of China (No. Y6090210), and the Qian-Jiang Talents Project of Zhejiang Province (No. 2010R10102).

-
- [1] J. Lukasik *et al.*, Phys. Lett. B **608**, 223 (2005) [arXiv:nucl-ex/0410030].
 - [2] A. Andronic, J. Lukasik, W. Reisdorf and W. Trautmann, Eur. Phys. J. A **30**, 31 (2006) [arXiv:nucl-ex/0608015].
 - [3] W. Reisdorf *et al.* [FOPI Collaboration], Nucl. Phys. A **781**, 459 (2007) [arXiv:nucl-ex/0610025].
 - [4] W. Reisdorf *et al.* [FOPI Collaboration], arXiv:1005.3418 [nucl-ex].
 - [5] P. Danielewicz, R. Lacey and W. G. Lynch, Science **298**, 1592 (2002) [arXiv:nucl-th/0208016].
 - [6] J. Lukasik *et al.*, the INDRA and ALADIN Collaborations, unpublished.
 - [7] D. J. Magestro, W. Bauer and G. D. Westfall, Phys. Rev. C **62**, 041603 (2000).
 - [8] B. A. Li, L. W. Chen and C. M. Ko, Phys. Rept. **464**, 113 (2008) [arXiv:0804.3580 [nucl-th]].
 - [9] C. Fuchs, J. Phys. G **35**, 014049 (2008).
 - [10] C. Hartnack, H. Oeschler and J. Aichelin, Phys. Rev. Lett. **96**, 012302 (2006) [arXiv:nucl-th/0506087].

- [11] P. Danielewicz, *Annals Phys.* **152**, 239 (1984).
- [12] P. Danielewicz, *Annals Phys.* **152**, 305 (1984).
- [13] K. C. Chou, Z. B. Su, B. L. Hao and L. Yu, *Phys. Rept.* **118**, 1 (1985).
- [14] G. Mao, Z. Li, Y. Zhuo, Y. Han and Z. Yu, *Phys. Rev. C* **49**, 3137 (1994).
- [15] Q. Li, Z. Li and G. Mao, *Phys. Rev. C* **62**, 014606 (2000) [arXiv:nucl-th/0005012].
- [16] G. F. Bertsch, W. G. Lynch and M. B. Tsang, *Phys. Lett. B* **189**, 384 (1987).
- [17] R. C. Lemmon, *et al.*, *Phys. Lett. B* **446**, 197 (1999).
- [18] D. Cussol *et al.*, *Phys. Rev. C* **65**, 044604 (2002).
- [19] G. Lehaut *et al.* [INDRA-ALADIN Collaboration], *Phys. Rev. Lett.* **104**, 232701 (2010).
- [20] Y. Zhang, Z. Li and P. Danielewicz, *Phys. Rev. C* **75**, 034615 (2007).
- [21] G. Mao, Z. Li, Y. Zhuo, Y. Han, Z. Yu and M. Sano, *Z. Phys. A* **347**, 173 (1994).
- [22] G. Giansiracusa, U. Lombardo and N. Sandulescu, *Phys. Rev. C* **53**, R1478 (1996).
- [23] Q. Li, Z. Li and E. Zhao, *Phys. Rev. C* **69**, 017601 (2004).
- [24] F. Sammarruca, arXiv:nucl-th/0506081.
- [25] F. Sammarruca and P. Krastev, arXiv:nucl-th/0509011.
- [26] Q. Li, Z. Li, S. Soff, M. Bleicher and H. Stoecker, *J. Phys. G* **32**, 407 (2006) [arXiv:nucl-th/0601047].
- [27] P. Danielewicz, B. Barker and L. Shi, *AIP Conf. Proc.* **1128**, 104 (2009) [arXiv:0903.2560 [nucl-th]].
- [28] Q. Li, C. Shen and M. Di Toro, *Mod. Phys. Lett. A* **25**, 669 (2010) [arXiv:0908.2825 [nucl-th]].
- [29] B. A. Li and L. W. Chen, *Phys. Rev. C* **72**, 064611 (2005).
- [30] G. Q. Li and R. Machleidt, *Phys. Rev. C* **48**, 1702 (1993) [arXiv:nucl-th/9307028].
- [31] G. Q. Li and R. Machleidt, *Phys. Rev. C* **49**, 566 (1994) [arXiv:nucl-th/9308016].
- [32] S. A. Bass *et al.*, [UrQMD-Collaboration], *Prog. Part. Nucl. Phys.* **41**, 255 (1998).
- [33] M. Bleicher *et al.*, [UrQMD-Collaboration], *J. Phys. G: Nucl. Part. Phys.* **25**, 1859 (1999).
- [34] E. L. Bratkovskaya *et al.*, *Phys. Rev. C* **69**, 054907 (2004).
- [35] Q. Li, Z. Li, S. Soff, R. K. Gupta, M. Bleicher and H. Stoecker, *J. Phys. G* **31**, 1359 (2005) [arXiv:nucl-th/0507068].
- [36] Q. Li, Z. Li, E. Zhao and R. K. Gupta, *Phys. Rev. C* **71**, 054907 (2005) [arXiv:nucl-th/0504065].

- [37] Q. Li, Z. Li, S. Soff, M. Bleicher and H. Stoecker, J. Phys. G **32**, 151 (2006) [arXiv:nucl-th/0509070].
- [38] Q. Li and M. Bleicher, J. Phys. G **36**, 015111 (2009) [arXiv:0808.3457 [nucl-th]].
- [39] H. Petersen, Q. Li, X. Zhu and M. Bleicher, Phys. Rev. C **74**, 064908 (2006) [arXiv:hep-ph/0608189].
- [40] Y. Yuan, Q. Li, Z. Li and F. H. Liu, Phys. Rev. C **81**, 034913 (2010) [Erratum-ibid. C **81**, 069901 (2010)] [arXiv:1002.4905 [nucl-th]].
- [41] W. Trautmann *et al.*, Prog. Part. Nucl. Phys. **62**, 425 (2009) [arXiv:0904.3495 [nucl-ex]].
- [42] W. Trautmann *et al.*, Nucl. Phys. A **834**, 548C (2010) [Int. J. Mod. Phys. E **19**, 1653 (2010)] [arXiv:1001.3867 [nucl-ex]].
- [43] Q. Li, M. Bleicher and H. Stoecker, Phys. Lett. B **659**, 525 (2008) [arXiv:0709.1409 [nucl-th]].
- [44] Q. Li, M. Bleicher and H. Stoecker, Phys. Lett. B **663**, 395 (2008) [arXiv:0802.3618 [nucl-th]].
- [45] J. Aichelin and H. Stöcker, Phys. Lett. B **176**, 14 (1986).
- [46] J. Aichelin, Phys. Rept. **202**, 233 (1991).
- [47] H. Sorge, H. Stöcker and W. Greiner, Annals Phys. **192**, 266 (1989).
- [48] S. A. Bass *et al.*, Phys. Rev. Lett. **81**, 4092 (1998).
- [49] <http://th.physik.uni-frankfurt.de/~urqmd>; H. Petersen, M. Bleicher, S. A. Bass and H. Stöcker, arXiv:0805.0567 [hep-ph].
- [50] C. Hartnack, R. K. Puri, J. Aichelin, J. Konopka, S. A. Bass, H. Stoecker and W. Greiner, Eur. Phys. J. A **1**, 151 (1998) [arXiv:nucl-th/9811015].
- [51] B. A. Li, Phys. Rev. Lett. **88**, 192701 (2002) [arXiv:nucl-th/0205002].
- [52] B. A. Brown, Phys. Rev. Lett. **85** (2000) 5296.
- [53] M. A. Famiano *et al.*, Phys. Rev. Lett. **97**, 052701 (2006) [arXiv:nucl-ex/0607016].
- [54] M. B. Tsang, Y. Zhang, P. Danielewicz, M. Famiano, Z. Li, W. G. Lynch and A. W. Steiner, Phys. Rev. Lett. **102**, 122701 (2009) [Int. J. Mod. Phys. E **19**, 1631 (2010)] [arXiv:0811.3107 [nucl-ex]].
- [55] S. A. Bass, C. Hartnack, H. Stöcker and W. Greiner, Phys. Rev. C **51**, 3343 (1995).
- [56] M. Isse, A. Ohnishi, N. Otuka, P. K. Sahu and Y. Nara, Phys. Rev. C **72**, 064908 (2005).
- [57] R. Brockmann and R. Machleidt, Phys. Rev. C **42**, 1965 (1990).
- [58] F. Hofmann, C. M. Keil and H. Lenske, Phys. Rev. C **64**, 034314 (2001) [arXiv:nucl-th/0007050].

- [59] C. Fuchs, A. Faessler and M. El-Shabshiry, Phys. Rev. C **64**, 024003 (2001) [arXiv:nucl-th/0103057].
- [60] H. Kruse, B. V. Jacak, J. J. Molitoris, G. D. Westfall and H. Stoecker, Phys. Rev. C **31**, 1770 (1985).
- [61] Q. Li, Mod. Phys. Lett. A **24**, 41 (2009) [arXiv:0808.0624 [nucl-th]].
- [62] W. Reisdorf *et al.* [FOPI Collaboration], Phys. Rev. Lett. **92**, 232301 (2004) [arXiv:nucl-ex/0404037].